Effects of Silicide Inclusion Shape on Thermal Transport of Silicon-based Nanowires and Nanocomposites for Thermoelectric Applications

Laia Ferrer-Argemi, Jonathan Sullivan, and Jaeho Lee Mechanical and Aerospace Engineering University of California, Irvine Irvine, CA, 92697 USA Email: jaeholee@uci.edu

ABSTRACT

Efficient silicon-based thermoelectric materials compatible with the existent electronic technology would provide excellent on-chip cooling opportunities. However, the high thermal conductivity of silicon has historically limited its thermoelectric performance. Here, we demonstrate the high potential of silicon-based nanocomposites by fabricating silicon nanowires with nickel silicide nanoinclusions with a scalable and economic sintering process. Preliminary measurements of the thermal conductivity of single nanowires from 40 to 325 K show a reduction of the thermal conductivity of a factor of 4 compared to silicon nanowires of the same length. We demonstrate that this reduction is probably a due to an increased phonon scattering with the inclusions, which grow epitaxially and form rhombohedral shapes. In order to better predict the thermal conductivity with non-spherical shapes, we combine ray tracing simulations and classical transport theories to demonstrate that the thermal conductivity reduction can be maximized by using elongated inclusion shapes (i.e. triangles or T-shapes) with small neck sizes. The findings of this work expand the understanding of transport phenomena in complex nanoengineered materials and open promising optimization paths for silicon-based thermoelectric materials.

KEYWORDS: heat transfer, low-temperature measurements, nanowires, nanocomposites, silicide, thermal conductivity, electroless deposition, thermometry techniques.

NOMENCLATURE

R Resistance, Ω A area, m^2

T temperature, K I current, A

S Seebeck coefficient, VK⁻¹

L length, m

k_B Boltzmann constant, m²kgs⁻²K⁻¹

n phonon mode *N* phonon population

ħ reduced plank constant, m²kgs⁻¹

f shape factor

 f_{BE} Bose-Einstein distribution

 v_g phonon group velocity

D phonon density of statesd nanowire diameter

r inclusion characteristic length

R_B boundary resistance

Greek symbols

κ thermal conductivity, Wm⁻¹K⁻¹
σ electrical conductivity, Sm⁻¹

 \mathcal{T} transmission coefficient

ω phonon angular frequency, rad/s

 Λ mean free path τ relaxation time

Subscripts

NW nanowire D domain

U Umklapp Imp impurity

B boundary L longitudinal

T transversal m matrix

p particle

INTRODUCTION

Silicon-based nanocomposites are attractive thermoelectric materials due to the abundance of the constituent elements, high melting point, and compatibility with electronic and photovoltaic technologies.[1]-[3] Bulk silicon compounds such as higher manganese silicides (HMS), MgSi₂, β-FeSi₂, and SiGe present high thermoelectric figure of merit (zT) primarily because of low thermal conductivity and high Seebeck coefficient.[4]–[7] However, bulk materials $zT = \frac{\sigma S^2}{\kappa} T$ is limited by the intrinsic interdependence of the electrical conductivity σ , Seebeck coefficient S, and thermal conductivity κ . Composite materials can overcome this limitation by inducing phonon scattering without significantly affecting phonon transport. Moreover, metal inclusions in a semiconductor matrix produce a Schottky barriers[8], [9] at the interface, which can enhance the power factor (σS^2) by filtering low energy electrons.[10], [11]

The contribution of the inclusions to the composite's effective thermal conductivity depends on the inclusion material intrinsic thermal conductivity and the thermal boundary resistance between the inclusion and the matrix material.[12] Although the mechanisms that drive the thermal boundary resistance are still not fully understood, the Diffuse Mismatch Model (DMM)[12] has been shown to be a reasonably good approximation for experimental values between greatly acoustically mismatched materials,[13] and epitaxial silicon-silicide boundaries.[14] Recent thermography measurements have shown that the DMM might overestimate the phonon transmission at intermediate frequencies especially if the interface is not oxide free.[15] The inclusion distribution and shape also affect the effective thermal conductivity.[16], [17] Previously reported thermal conductivity analytical expressions[18] and effective medium theories[19] (EMTs) are derived for ellipsoidal or squared inclusions and layered structures. However, recent advancements in nanomaterial

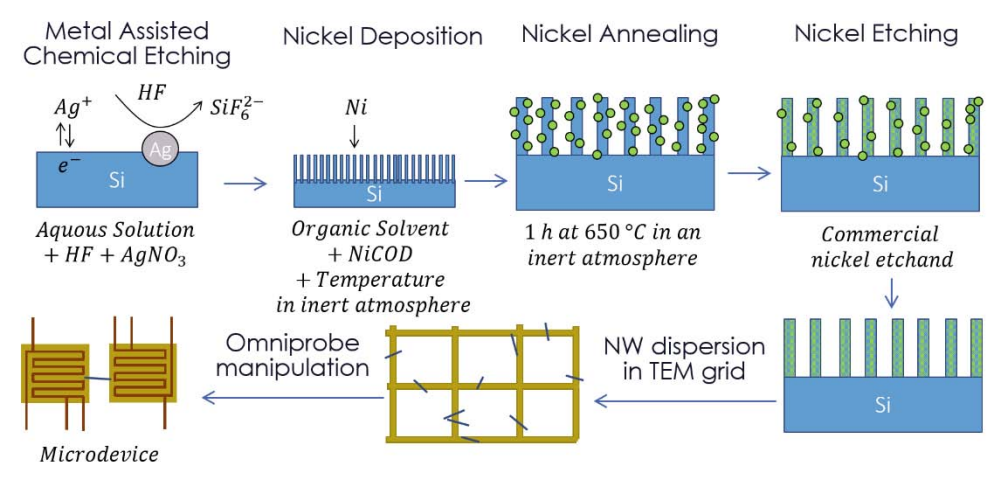


Fig. 1. Process layout of the sample preparation from the initial Si wafer to a single nanowire bonded into the measurement microdevice.

synthesis show that epitaxially grown silicide inclusions in silicon have a rhombohedral shape,[20] the thermal conductivity of which cannot be captured by the aforementioned expressions and EMTs.[16] This calls for an improved method, such as the ray tracing technique, to be incorporated into the investigation of phonon transport in nanocomposites with non-elliptical inclusion shapes.

In this work, we have fabricated Si nanowires with nickel silicide inclusions (Si-NiSi₂ NWs) and present thermal conductivity measurements of a single wire. Since the nickel self-propagates through the silicon wires when sufficient heat is applied, the resulting inclusions are epitaxially grown and with a rhombohedral shape. In order to better predict the thermal conductivity of such structure, we use Monte Carlo ray tracing simulations to compare the thermal conductivity given by different inclusion shapes and the parameters that affect it. The results presented here show that efficient silicon-based thermoelectrics can be achieved by engineering silicide inclusions and open new exiting paths of investigation.

SAMPLE PREPARATION

The nanowire preparation process layout is schematized in Fig. 1. The main steps are metal assisted chemical etching

(MACE) to create a silicon nanowire forest with controlled dimensions, electroless deposition of nickel, annealing of the sample, etching of the residual nickel for 30 minutes, dispersion of the nanowires into a TEM grid, and manipulation of a single wire using a SEM omniprobe to place it in the microdevice.

Si NW Forest Fabrication

We follow the procedure detailed by Hochbaum et al. [21] to fabricate a large scale Si NW forest. Briefly, a Si wafer is cleaned by immersing it successively and during 10 minutes in an acetone, IPA, and DI water. This wafer in then placed in 500 ml of aqueous solution of 0.02M AgNO₃ and 5M Hydrofluoric Acid, which etches the silicon randomly and creates a nanowire forest. The mechanism driving the MACE of silicon is described in detail in the literature,[22] being the main factors driving the nanowire diameter, in order of importance, the HF concentration, the Ag concentration, and the reaction temperature.[23] The diameter of the wires obtained using the above conditions ranges between 20 and 250 nm, while the length depends on the etching time. We achieve 50 µm in 5 h. The wafer is then placed in a nitric acid solution for 30 minutes and transferred to a clean nitric acid solution for another 30

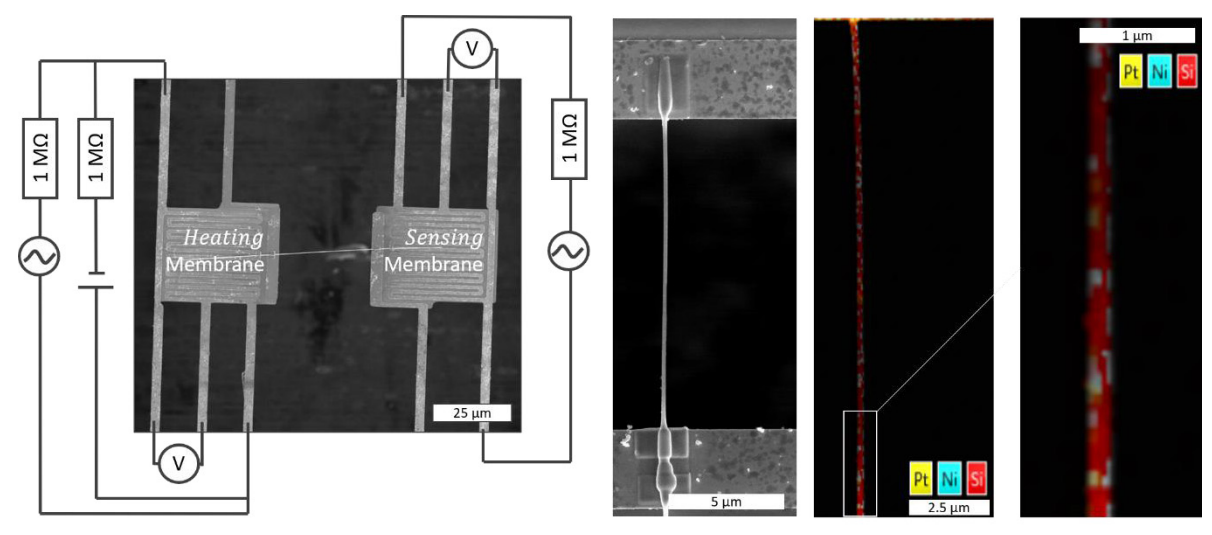


Fig. 2, (A) Connection schematics to the microdevice. (B) Top-view SEM image of the measured sample of 14.1 µm long and 170 nm of diameter. (C) EDS mapping of the measured sample including Pt (yellow), Ni (blue), and Si (red). The measured inclusion density is 30 %.

minutes to remove the silver particles. Then, the wafer is placed in IPA for 1 h.

Ni-SiNi NW Fabrication

To create the NiSi₂ inclusions, we first use electroless deposition to randomly deposit nanometric nickel particles in the Si NW forest. To deposit in a small area that fits in a scintillation vial, we mix 25 mg of Ni(COD)₂ with 5 ml of toluene in an oxygen free atmosphere. For bigger containers to fit larger pieces, use enough toluene to submerge the wafer while maintaining the Ni(COD)₂ concentration. We seal the vial and place it in a hot plate at 70 °C for 1 h. The wafer piece is then placed in a tube furnace at 650 °C for 1 h in inert atmosphere and cooled down convectively. Any potential residual nickel is etched away using commercial nickel etchant. Sample Preparation

The wafer piece with Si-NiSi₂ NW forest is placed in a scintillation vial with IPA and sonicated for 10 minutes to disperse the wires. A couple of drops of IPA with dispersed wires are placed in a TEM grid and transferred to the SEM (Quanta) to be examined. When we locate a wire of the desired dimensions and that is in the right position, we use the Omniprobe to transfer it to the microdevice used for thermal conductivity measurements and bonded using platinum deposition. The sample reported in this study can be seen in Fig. 2 bonded to the microdevice.

METHODOLOGY

Thermal Conductivity Measurements

The sample dimensions are measured using high resolution SEM (Magellan) imaging and its composition is measured using EDS parterning as seen in Fig. 2. The measuring circuit is detailed in Fig. 3 and the procedure has been described in

detail in the literature. [21], [24] Briefly, a microdevice with two suspended membranes is used to measure the thermal conductivity of the wire by heating one membrane up and measuring the resulting temperature rise in the other (sensing) membrane. The sample is bonded using wire bonding (WestBond) and placed in a high-vacuum cryostat (JANIS VPF-800) that allows temperatures down to 4 K. We use a lockin amplifier (SR830) to accurately measure the resistance of the membranes and its change with applied current. A power supply is used to significantly increase the temperature of the heating membrane up to 25 K. An accurate measurement of the resistance change with temperature is crucial for the measurement of the thermal conductivity [25], [26]. To precisely measure how the resistance of the membranes changes with temperature, we use a Lake Shore 330 to control the temperature of the vacuum chamber within 30 mK and a radiation shield to minimize radiation losses.

Modeling

We perform Monte-Carlo ray tracing to capture the impact of inclusion shapes seen in Fig. 3 on the phonon mean free path due to boundary scattering at the inclusion interfaces, Λ_B .[16], [27] Briefly, we combine Landauer formalism[28], [29] and kinetic theory[30] to convert the frequency-dependent phonon transmission coefficient $\langle \mathcal{T}(\omega) \rangle$ given by ray tracing simulations to Λ_B as

$$\Lambda_B = \frac{3L_D \langle \mathcal{T}(\omega) \rangle}{4f}$$

where L_D is the simulation length and f is the shape factor detailed in Table 1. The thermal conductivity is then computed as

Shape #	Inclusion density 25%		P = 100 [nm]	
1	Squares	N	50	
		L	50	
2	Circles	N	43.6	
		L	56.4	
3	Hexagons	N	38	
		L	31	
4	Diamonds	N	29.3	
		L	50	
5	Triangles	N	29	
		L	78.9	
6	Ts	N	29	
		L	20.59	
7	Us	N	29	
		L	20.59	
8	Equilateral	N	24	
	Triangles	L	76	
9	Ts	N	22	
		L	18.76	

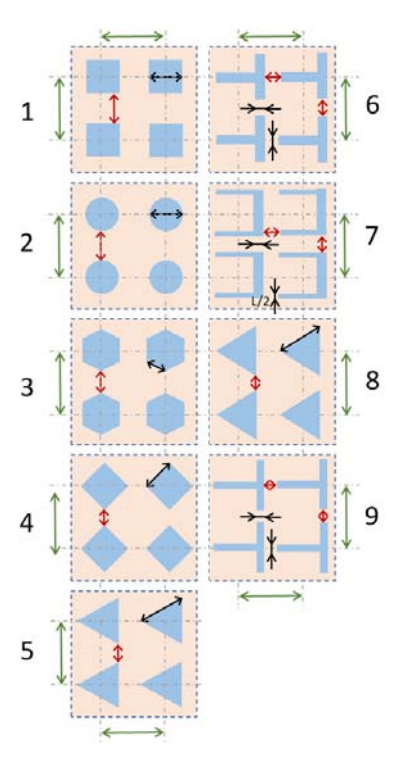


Fig. 3. Schematics of the unit cells of the studied geometries with the relevant dimensions, each one is assigned an identification number that is used in the results section to refer to each geometry.

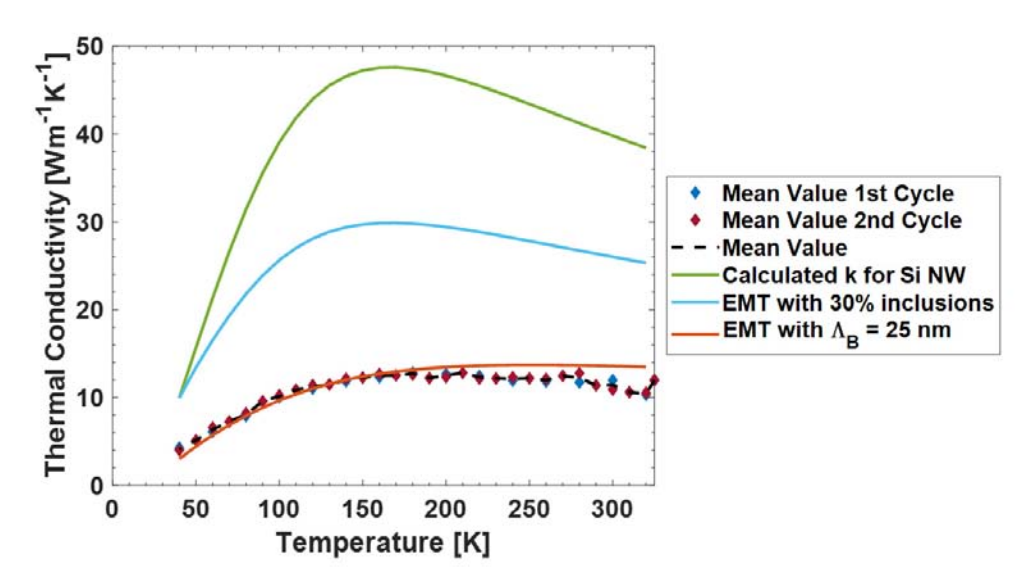


Fig. 4. Measured thermal conductivity of the Si-NiSi NW shown in Fig. 2 ($L=14.1~\mu m$ and d=180~nm) across two temperature cycles from 325 to 40 K (diamonds). Calculated thermal conductivity of a Si NW of the same dimensions yielding a boundary mean free path of 118.7 nm (green), a Si NW with 30 % NiSi2 inclusion density without further boundary scattering (blue), and with increased boundary scattering due to inclusions down to 25 nm (orange). The decreasing trend above room temperature indicates effects not covered by our modeling.

$$\kappa = \frac{1}{6\pi^2} \sum_n \int \hbar \omega \frac{\partial f_{BE}}{\partial T} v_g(\omega,n) [\Lambda_B^{-1} + \Lambda_{bulk}^{-1}(\omega,n)]^{-1} D(\omega,n) d\omega.$$

We use full phonon dispersion relations by taking a quadratic fit of the experimental data for each acoustical branch of Si [31] NiSi_{2.}[32]. The different phonon scattering mechanisms are combined via Matthiessen's rule under relaxation time approximation, in which $\Lambda = \tau v$ and $\tau^{-1} =$ $\tau_b^{-1} + \tau_U^{-1} + \tau_{imp}^{-1}$, where the subscripts denote phononboundary, -Umklapp, and -impurity scattering, respectively. We use the expressions of relaxation time detailed previously[27] to compute Umklapp and impurity scatterings, which are $\tau_U^{-1} = P\omega^2 T \exp\left(-\frac{c_U}{T}\right)$ and $\tau_{imp}^{-1} = C_I\omega^4$, where $P = 1.53 \times 10^{-19} \frac{\text{s}}{\text{K}}$, $C_U = 144 \text{ K}$, and $C_I = 2.54 \times 10^{-45} \text{ s}^3$. The impurity scattering parameter corresponds to a 10^{15} cm⁻³ boron-doped silicon with an electrical conductivity of 5.84 \pm 1.3 S/m.[27] Boundary scattering includes scattering with inclusions and, in the case of nanowires, longitudinal and transversal scattering, which can be estimated as $\Lambda_{B,L}^{-1} = \frac{4}{\pi L_{NW}}$ and $\Lambda_{B,T}^{-1} = \frac{3}{2d_{NW}}$, respectively. Phonons are introduced into the simulation with a random frequency according to the phonon population distribution at each temperature. Different approaches are used throughout the literature to compute the thermal boundary resistance; [33] in this study, we use the DMM because diffuse scattering is more likely to occur above 10 K for the studied material-pairs and it has been seen to be a good approximation between silicon and silicide epitaxial interfaces.[13]–[15]

Table 1. Shape factor used for geometries 1 to 5

Squares	Circles	Hexagons	Diamonds	Triangles
1.1	1.03	1.06	1.14	1.19

According to the DMM, the phonon probability to get transmitted from material A to B upon collision with a boundary is computed as [33]-[35]

$$t_{AB}(\omega) = \frac{\sum_{n} v_{i,B} N_{i,B}(\omega,T)}{\sum_{n} v_{i,A} N_{i,A} + \sum_{n} v_{i,B} N_{i,B}},$$

where $N = f_{BE}D$ is the phonon population at each frequency. Using the quadratic fit to the complete phonon dispersion relation, we can overcome the Debye approximation and obtain more accurate results.[30], [34], [35] Note that the transmission coefficient t_{AB} does not depend on the temperature if both materials A and B are at the same temperature. After the collision, a new direction is randomly assigned within the resulting material.[33]

EXPERIMENTAL RESULTS

Two measurement cycles between 325 and 40 K were performed on the sample shown in Fig. 2. In each cycle we performed 5 measurements to obtain the average thermal conductivity at each temperature. As seen in Fig. 4, the thermal conductivity of the Si-NiSi NWs is much lower than that of a Si NW with similar dimensions. In order to include the effect of the NiSi inclusions, we start by using Hasselman and Johnson effective medium theory to compute the effective thermal conductivity of the composite material

$$\frac{\kappa_{eff}}{\kappa_{m}} = \frac{\left(\frac{\kappa_{p}}{\kappa_{m}} - \frac{\kappa_{p}R_{B}}{r} - 1\right)\phi + \left(\frac{\kappa_{p}}{\kappa_{m}} + \frac{\kappa_{p}R_{B}}{r} + 1\right)}{\left(1 + \frac{\kappa_{p}R_{B}}{r} - \frac{\kappa_{p}}{\kappa_{m}}\right)\phi + \left(\frac{\kappa_{p}}{\kappa_{m}} + \frac{\kappa_{p}R_{B}}{r} + 1\right)}$$

where the inclusion density is determined using EDS and image processing to be around 30 %, and the nickel silicide thermal conductivity is assumed to not change significantly from the 10.3 Wm⁻¹K⁻¹ value reported at room temperature.[36] However, the effective approach still predicts a much larger

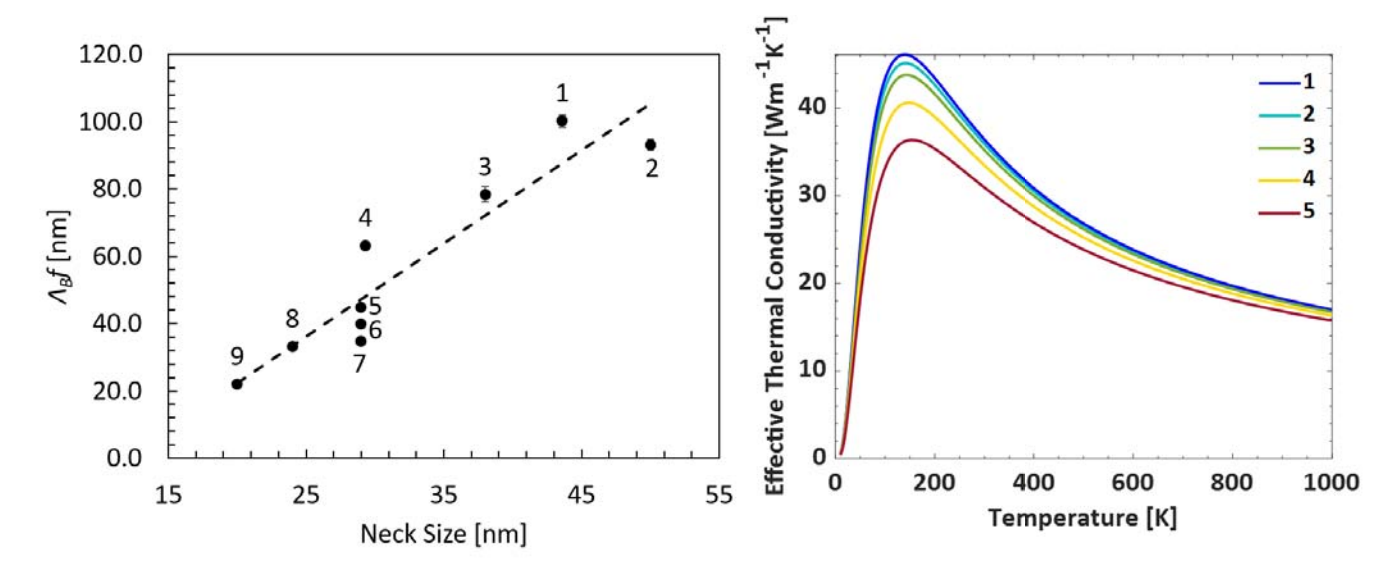


Fig. 5. (A) Ray tracing results with the different geometries detailed in Fig 3 for Si nanoporous structures. (B) Effective thermal conductivity with 25% nickel silicide inclusions and the indicated geometries. Geometries that require a smaller neck size to maintain the inclusion density result in lower thermal conductivities.

thermal conductivity than the experimental results. We have to reduce the average boundary scattering to only 25 nm to reach the measured thermal conductivity values. The increased scattering might be due to two contributions. The first contribution might come from the NW roughness. Several studies in the literature have presented reduced thermal conductivity of Si NWs prepared with MACE and have correlated the reduced thermal conductivity to surface roughness of the NW.[21], [24], [37] The second contribution to the thermal conductivity reduction comes from the inclusions, which block the path of the phonons and increase the boundary scattering. In order to better predict the thermal conductivity given non-spherical inclusions, we perform Monte Carlo ray tracing simulations in the next section to understand the implications of different inclusion shapes.

In addition, we observe a descending trend above room temperature that cannot be explained with the current framework, where the boundary scattering dominates the thermal transport and saturates the thermal conductivity (see orange line in Fig. 4). Possibly, electron-phonon coupling at the interface causes extra scattering or NiSi₂ thermal conductivity starts to decrease, but further measurements at higher temperatures and different inclusion densities are needed to confirm these hypotheses.

SIMULATION RESULTS

We first analyze the effect of different inclusion shapes in a silicon nanoporous media using the results given by ray tracing. In order to isolate the effect of the inclusion shape on the probability for a phonon to get transmitted, we look into the product of the boundary mean free path and the shape factor. As seen in Fig. 5 and previously noted by different authors,[16], [38] the boundary mean free path tends to decrease with decreasing neck size. However, as seen in the results from geometries 4 to 8, which have all a neck size around 29 nm, the elongation of the shape (length in the flux direction) and the blockage of possible transmission paths seems to further

increase the boundary mean free path. We are currently investigating how the different parameters drive the boundary mean free path reduction.

We also show the resulting effective thermal conductivity with 25% nickel silicide inclusions and geometries 1 to 5. The shape factor, which is computed by solving the Fourier equation with each geometry, is detailed in Table 1. As indicated by the results in Fig 5A, geometries such as triangles and hexagons result in a lower thermal conductivity. Indeed, the thermal conductivity reduction is significant, especially around 200 K, despite the constant inclusion density. However, since the inclusions in our samples have different sizes, a detailed simulation including different inclusion sizes might be necessary to obtain an accurate prediction for each sample.

CONCLUSIONS

We fabricated Si NWs with random nickel silicide inclusions as promising thermoelectric materials. Preliminary data shows a thermal conductivity reduction of a factor of 4 compared to Si NWs with the same dimensions. This NWs are also an ideal scenario to study the electron-phonon coupling at the interface and its dependence on temperature. Our modeling shows that an increased phonon boundary scattering is necessary for the NWs to reach such low thermal conductivity values, which is provided by the inclusions. We have shown that rhombohedral shapes are contributing to the reduction of the phonon boundary mean free path, but due to the random nature of the inclusions, a detailed study of each sample might be necessary to before discarding other possible scattering mechanisms.

Acknowledgments

The authors are grateful to Dr. J. P. Fleurial, Dr. S. Bux, Dr. Hochbaum, and Dr. G. Cerretti for valuable discussions and to Prof. G. Wehmeyer and Z. Yu for his help with the early development of the ray tracing model. This work was in part supported by National Science Foundation (ECCS-1807825). SEM work was performed at the UC Irvine Institute (LEXI).

References

- [1] N. Mingo, D. Hauser, N. P. Kobayashi, M. Plissonnier, and A. Shakouri, "Nanoparticle-in-alloy approach to efficient thermoelectrics: Silicides in SiGe," *Nano Lett.*, vol. 9, no. 2, pp. 711–715, 2009.
- [2] L. J. Chen, "Metal silicides: An integral part of microelectronics," *The Journal of The Minerals, Metals & Materials Society*, vol. 57, no. 9. pp. 24–30, 2005.
- [3] M. Seibt, H. Hedemann, A. A. Riedel, F. Istratov, A. Sattler, and W. Schroeter, "Structural and Electrical Properties of Metal Silicide Precipitates in Silicon," *Phys. Status Solidi*, vol. 171, no. 1, pp. 301–310, 1999.
- [4] C. B. Vinning, "Thermoelectric Properties of Silicides," *CRC Handbook of Thermoeletrics*. pp. 277–286, 1995.
- [5] A. Nozariasbmarz, A. Agarwal, Z. A. Coutant, M. J. Hall, J. Liu, R. Liu, A. Malhotra, P. Norouzzadeh, M. C. Öztürk, V. P. Ramesh, Y. Sargolzaeiaval, F. Suarez, and D. Vashaee, "Thermoelectric silicides: A review," *Jpn. J. Appl. Phys.*, vol. 56, p. 05DA04, 2017.
- [6] G. Joshi, H. Lee, Y. Lan, X. Wang, G. Zhu, D. Wang, R. W. Gould, D. C. Cuff, M. Y. Tang, M. S. Dresselhaus, G. Chen, and Z. Ren, "Enhanced thermoelectric figure-of-merit in nanostructured p-type silicon germanium bulk alloys," *Nano Lett.*, vol. 8, no. 12, pp. 4670–4674, 2008.
- [7] I. Opahle, A. Parma, E. J. McEniry, R. Drautz, and G. K. H. Madsen, "High-throughput study of the structural stability and thermoelectric properties of transition metal silicides," *New J. Phys.*, vol. 15, p. 105010, 2013.
- [8] J. Tersoff, "Schottky Barrier Heights and the Continuum of Gap States," *Phys. Rev. Lett.*, vol. 52, no. 6, p. 465, 1984.
- [9] J. P. Gambino and E. G. Colgan, "Silicides and ohmic contacts," *Mater. Chem. Phys.*, 1998.
- [10] J. M. O. Zide, D. Vashaee, Z. X. Bian, G. Zeng, J. E. Bowers, A. Shakouri, and a. C. Gossard, "Demonstration of electron filtering to increase the Seebeck coefficient in In0.53Ga0.47As/In0.53Ga0.28Al0.19As superlattices," *Phys. Rev. B*, vol. 74, p. 205335, 2006.
- [11] M. Zebarjadi, K. Esfarjani, A. Shakouri, J.-H. Bahk, Z. Bian, G. Zeng, J. Bowers, H. Lu, J. Zide, and A. Gossard, "Effect of nanoparticle scattering on thermoelectric power factor," *Appl. Phys. Lett.*, vol. 94, p. 202105, 2009.
- [12] E. Swartz and R. Pohl, "Thermal boundary resistance," *Rev. Mod. Phys.*, vol. 61, no. 3, pp. 605–668, 1989.
- [13] H. K. Lyeo and D. G. Cahill, "Thermal conductance of interfaces between highly dissimilar materials," *Phys. Rev. B Condens. Matter Mater. Phys.*, vol. 14, no. 8, p. 144301, 2006.
- [14] N. Ye, J. P. Feser, S. Sadasivam, T. S. Fisher, T. Wang, C. Ni, and A. Janotti, "Thermal transport across metal silicide-silicon interfaces: An experimental comparison between epitaxial and nonepitaxial interfaces," *Phys. Rev. B*, vol. 95, no. 8, p. 08543, 2017.
- [15] C. Hua, X. Chen, N. K. Ravichandran, and A. J. Minnich, "Experimental metrology to obtain thermal

- phonon transmission coefficients at solid interfaces," *Phys. Rev. B*, vol. 95, p. 205423, 2017.
- [16] Z. Yu, L. Ferrer-Argemi, and J. Lee, "Investigation of thermal conduction in symmetric and asymmetric nanoporous structures," *J. Appl. Phys.*, vol. 122, no. 24, p. 244305, 2017.
- [17] D. Chakraborty, S. Foster, and N. Neophytou, "Monte Carlo phonon transport simulations in hierarchically disordered silicon nanostructures," *Phys. Rev. B*, 2018.
- [18] A. Minnich and G. Chen, "Modified effective medium formulation for the thermal conductivity of nanocomposites," *Appl. Phys. Lett.*, vol. 91, p. 073105, 2007.
- [19] K. Pietrak and T. S. Winiewski, "A review of models for effective thermal conductivity of composite materials," *Open Access J. J. Power Technol.*, vol. 95, no. 1, pp. 14–24, 2015.
- [20] F. Panciera, Y. C. Chou, M. C. Reuter, D. Zakharov, E. A. Stach, S. Hofmann, and F. M. Ross, "Synthesis of nanostructures in nanowires using sequential catalyst reactions," *Nat. Mater.*, vol. 14, no. 8, p. 820, 2015.
- [21] A. I. Hochbaum, R. Chen, R. D. Delgado, W. Liang, E. C. Garnett, M. Najarian, A. Majumdar, and P. Yang, "Enhanced thermoelectric performance of rough silicon nanowires," *Nature*, vol. 451, pp. 163–167, 2008.
- [22] M. L. Zhang, K. Q. Peng, X. Fan, J. S. Jie, R. Q. Zhang, S. T. Lee, and N. B. Wong, "Preparation of large-area uniform silicon nanowires arrays through metalassisted chemical etching," *J. Phys. Chem. C*, vol. 112, no. 12, pp. 4444–4450, 2008.
- [23] C.-Y. Chen, C.-S. Wu, C.-J. Chou, and T.-J. Yen, "Morphological Control of Single-Crystalline Silicon Nanowire Arrays near Room Temperature," *Adv. Mater.*, vol. 20, pp. 3811–3815, 2008.
- [24] J. Lee, W. Lee, J. Lim, Y. Yu, Q. Kong, J. J. Urban, and P. Yang, "Thermal Transport in Silicon Nanowires at High Temperature up to 700 K," *Nano Lett.*, vol. 16, no. 7, pp. 4133–4140, 2016.
- [25] L. Ferrer-Argemi, A. Cisquella-Serra, M. Madou, and J. Lee, "Temperature-Dependent Electrical and Thermal Conductivity of Glassy Carbon Wires," *Proc.* 17th Intersoc. Conf. Therm. Thermomechanical Phenom. Electron. Syst. ITherm 2018, vol. 1, no. 1, pp. 1280–1288, 2018.
- [26] L. Ferrer-Argemi, E. S. Aliabadi, A. Cisquella-Serra, A. Salazar, M. Madou, and J. Lee, "Size-dependent electrical and thermal conductivities of electromechanically-spun glassy carbon wires," *Carbon N. Y.*, vol. 130, pp. 87–93, 2018.
- [27] J. Lee, W. Lee, G. Wehmeyer, S. Dhuey, D. L. Olynick, S. Cabrini, C. Dames, J. J. Urban, and P. Yang, "Investigation of phonon coherence and backscattering using silicon nanomeshes," *Nat. Commun.*, vol. 8, p. 14054, 2017.
- [28] S. Datta, *Electronic Transport in Mesoscopic Systems*, Revised Ed. Cambridge: Cambridge University Press, 1997.
- [29] C. Jeong, R. Kim, M. Luisier, S. Datta, and M. Lundstrom, "On Landauer versus Boltzmann and full

- band versus effective mass evaluation of thermoelectric transport coefficients," *J. Appl. Phys.*, vol. 107, no. 2, p. 023707, 2010.
- [30] N. Mingo, "Calculation of Si nanowire thermal conductivity using complete phonon dispersion relations," *Phys. Rev. B*, vol. 68, no. 11, p. 113308, 2003.
- [31] G. Dolling, "Lattice Vibrations in Crystals with the Diamond Structure," in *Proceedings of the Symposium on Inelastic Scattering of Neurons in Solids and Liquids*, Vol. 2., C. River, Ed. Vienna, 1963, pp. 37–48.
- [32] S. Sanguinetti, C. Calegari, and L. Miglio, "Phonon dispersion relations of metallic NiSi2 and CoSi2 by semi-empirical tight-binding calculation," *Appl. Surf. Sci.*, vol. 91, no. 1–4, pp. 103–106, 1995.
- [33] E. T. Swartz and R. O. Pohl, "Thermal boundary resistance," *Rev. Mod. Phys.*, vol. 61, no. 3, pp. 605–668, 1989.
- [34] P. Reddy, K. Castelino, and A. Majumdar, "Diffuse

- mismatch model of thermal boundary conductance using exact phonon dispersion," *Appl. Phys. Lett.*, vol. 87, no. 21, p. 211908, 2005.
- [35] L. De Bellis, P. E. Phelan, and R. S. Prasher, "Variations of Acoustic and Diffuse Mismatch Models in Predicting Thermal-Boundary Resistance," *J. Thermophys. Heat Transf.*, vol. 14, no. 2, pp. 144–150, 2000.
- [36] V. S. Neshpor, "The thermal conductivity of the silicides of transition metals," *J. Eng. Phys. Thermophys.*, vol. 15, no. 2, pp. 750–752, 1972.
- [37] P. Martin, Z. Aksamija, E. Pop, and U. Ravaioli, "Impact of phonon-surface roughness scattering on thermal conductivity of thin Si nanowires," *Phys. Rev. Lett.*, vol. 102, no. 2, p. 125503, 2009.
- [38] G. Romano and J. C. Grossman, "Phonon bottleneck identification in disordered nanoporous materials," *Phys. Rev. B*, vol. 96, no. 11, pp. 1–5, 2017.